Microelectronics Reliability 56 (2016) 170–181

Contents lists available at ScienceDirect

Microelectronics Reliability

journal homepage: www.elsevier.com/locate/mr

Lattice Boltzmann method study of bga bump arrangements on void formation

Aizat Abas [a,*], M.H.H. Ishak [a], M.Z. Abdullah [b], F. Che Ani [c], Soon Fuat Khor [a]

[a] School of Mechanical Engineering, Universiti Sains Malaysia, Engineering Campus, 14300 Nibong Tebal, Penang, Malaysia
[b] School of Aerospace Engineering, Universiti Sains Malaysia, Engineering Campus, 14300 Nibong Tebal, Penang, Malaysia
[c] Jabil Circuits, 56, Hilir Sungai Kluang 1, 11900 Bayan Lepas, Penang, Malaysia

ARTICLE INFO

Article history:
Received 11 July 2015
Received in revised form 8 September 2015
Accepted 14 October 2015
Available online 11 November 2015

Keywords:
Lattice Boltzmann method
Finite volume method
Capillary underfill
Air void
Ball grid array

ABSTRACT

This paper studies effects of different bump orientations on the void formation using Lattice Boltzmann method (LBM) based software. Prediction of air void is vital typically at the onset of reflow soldering which could reduce the reliability of the mold cavity. The effect of variations in pressure and velocity of the mold during flow on the formation of air voids are investigated for three different ball grid array (BGA) orientations namely perimeter, middle empty and full. The findings identified the predicted locations of void formation during the underfill encapsulation process. It was shown that middle empty orientation has the highest potential of void formation typically towards the end of mold flow as a result of low pressure and high velocity flow. In addition, using high bond number and high viscosity material could further reduce the air void formation.

1. Introduction

In the microelectronics industry, ball-grid-array (BGA) technology enables the design of integrate circuit (IC) packages with high volume of interconnection in a miniature size. Therefore, an inspection and evaluation of BGA is extremely important especially during underfilling process. The real world visualization on actual underfilling process is difficult and costly which led to the numerical simulation of the fluid flow through BGA. BGA technology gains industry-wide interest and commitment due to lowest cost package for high input/output (I/O) devices and lower pin count applications, achieve the six sigma assembly, and excellent electrical and thermal performance. Therefore, worldwide evaluation on BGA has accelerated in order to eliminate some perceived weakness. Many researchers have started the study on the application, advantages and disadvantages of BGA decades ago. Jay J. Liu et al. have done the overview of plastic ball grid array (PBGA) including the technical advantages, limitations, application area, the major hurdles for acceptance of PBGA and possible approaches to overcome these problems. The characteristics study includes package attributes, performance, reliability, solder joint fatigue, board routing, solder assembly yield, solder reparability and board delay [1].

The reliability issues of plastic flip packages are continuously investigated by the Paul S. Ho et al. through Moiré interferometry [2] and W.H Zhong et al. based on the effect of multiple reflow process [3]. The evolution of area-array interconnects with high input/output (I/0) count and power dissipation made thermal deformation an important reliability concern for flip chip packages. Therefore, Moiré interferometry has been proposed by Paul S. Ho et al. on the understanding of this thermo-behaviour of flip-chip packages. They disclose that underfilling process reduces the shear strains of the solder balls but leads to delamination of the underfill interfaces. Moire study also shows that the die-fillet corner is a critical region with local stress concentration in the package. Besides, the underfill above the through hole has a higher normal strain than other regions of underfill. The authors are looking forward to a better experimental methodology and computer modelling capability to ensure successful development of plastic area-array packages for the future. While W.H Zhong et al. examined the reliability of ball grid array (BGA) solder joints based on the effect of multiple reflow processes. The study is related to the mechanical behaviours and microstructures of BGA solder joints against organic solderability preservatives (OSP) coated copper pad on fibreglass (FR4) substrate after multiple reflow process. In this study, a new lead-free solder compound, Sb–3Ag–0.5Cu–8In (SACI) is compared with Sn–3Ag–0.5Cu (SAC) and Sn–37Pb (SP) solder. It was shown that the new lead-free SACI solder joints provide higher shearing strength compared to the SAC and SP joints during multiple reflow. However, the increase in number of reflow cycles does not significantly change the shearing force of these three types of solder joints. The fracture of SAC and SP solder joints occurred at the bulk solder whereas the fracture of SACI solder joints occurred in various combinations of bulk solder fracture, solder intermetallic (IMC) interface dissociation and pad/resin interface failure.

* Corresponding author.
E-mail address: aizatabas@usm.my (A. Abas).

http://dx.doi.org/10.1016/j.microrel.2015.10.014
0026-2714/

Underfill encapsulation process regularly suffers from incomplete filling or air voids. Many factors could have influenced the severity of void formation, for instance, ball grid array (BGA) orientations, dispensing type and the dimensions of the pitch and diameter of the BGA. Prior detection of air voids could increase package reliability typically during reflow process. Ranjit and Michael found out that air voids may lead to "popcorning" effect during the reflow process [4,5]. Stresses are build up during the reflow process leading to steam and development of vapour pressure. This vapour pressure in the air void region can lead to formation of dome-shape bulge and in time contributes to the development of crack. This cracking sound resembles the characteristic popcorn sound that will reduce the reliability of encapsulated package.

Several studies have been conducted using FVM based software, ANSYS, to determine the factors contributing to void formations. In a study by Zheng et al., prediction of air void is conducted during curing process for BCB bonding using experimental observations [6]. These voids if left undetected may degrade the bonding strength, reduce hermetic capability and in time may impact the yield and reliability of the package. Khor et al. found out that middle empty orientations contributed to highest void formation due to deformation of the center region and packed solder bumps [7]. Ernest et al. study the effect of microbump pitch on the formation of voids [8,9]. It was shown that air voids usually occur at the vicinity of microbump edge. Both studies are conducted on macro-scale level (finite volume method) without taking into account the effect of particle interaction forces on the micro-scale level. The air void formation requires deeper understanding of the strength attraction and repulsion at the particle level. It is the aim of this paper to take into account this effect using the so-called Lattice Boltzmann method (LBM). To the knowledge of the authors, no papers have been published that utilize LBM to solve and predict void formation problem. There are already few researches on fluid flow simulation through BGA in the past but they are mainly focused on finite volume method (FVM) and finite element method (FEM) [10]. A review on comparison between LBM and FVM proves the capability of another fluid flow simulation method which is LBM for BGA evaluation since LBM provides same accuracy as FVM on fluid flow simulation and better capability in dealing with instantaneous flows.

In recent years, LBM has been used extensively to model flow over obstacles and fluid–structure interaction problems with various applications in electronics, civil and biomedical fields. Many applications of LBM utilizes single component multiphase (SCMP) model [11,12]. The first implementation of SCMP on multiphase fluid uses the well-known Shan–Chen model [13–15]. The proposed approach is the so called "free energy" approach introduced by Swift et al. [16], and the "finite density" method that is combined with Enskog equation for application to dense gases [17,18]. Subsequently, a tracking energy based on temperature is introduced by Zhang and Chen [19,20]. These free energy and finite density models are highly influential in the development flow propagation and the interaction with obstacles due to consistent and more realistic treatment of equation of state in recovering the preserved essential (molecule) physics of the process. Following this development, Shan and Chen introduced pseudo-potential model for multi-component [21] and multiphase flow [13,22] (MCMP). It was a popular model based on collision operator that has been improved by long-range interaction force which imitates the pairwise interaction potential between dissimilar phases/components and impressive results are obtained with fairly little effort. The Shan–Chen model is therefore highly popular, despite potential numerical deficiencies in some areas. In this paper, the interaction between epoxy mold and solder bump is modelled based on Shan–Chen SCMP model given that it is highly effective in modelling multiphase flow problems and the particle–particle interaction forces are capable to fully capture the air voids formation.

2. Problem description

Electronic packaging (EP) is an enclosure and protective features to the electronic products. The process of fabrication, assembly and testing of EP may involve a lot of complex interaction with physical phenomena such as temperature, fluid flow, electromagnetic and stress. This project is related to 3-dimensional fluid flow simulation through a ball grid array (BGA). Fig. 1 depicts the schematic diagram of underfilling process for the flow. The BGA consists of square array of spherical balls across the surface attached to another piece of printed circuit board (PCB). The underfilling process will be simulated using Palabos which is based on LBM theory.

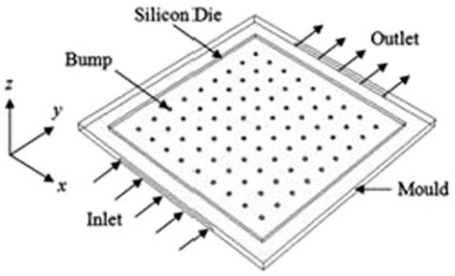

Fig. 1. Schematic diagram of flip-chip boundary conditions.

Fig. 2 shows the underfilling process involving the dispensing process of controlling the amount of material into the gap between the chip and substrate. The underfill encapsulation of ball grid array (BGA) is important in protecting and increasing reliability of the electronic packaging (EP) as it can reduce the global thermal expansion, stresses and strains between the silicon chip and substrate. The gap between the chip and silicon has to be completely filled with underfill material (underfill material flow correctly) in order to protect life of the chip assembly [23].

3. Governing equations

3.1. Lattice Boltzmann formulation

The results shown in this section are formulated using D3Q19 lattice model. In LBM, statistical description is used to explain the distribution function of particles and can be summarized in Eq. (1):

$$f(r + cdt, c + Fdt, t + dt) - f(r, c, t) = \Omega[f(r, c, t)], \tag{1}$$

where $f(r+cdt, c+fdt, t+dt)$ represents the distribution function of the molecules. The distribution function will determine the number of molecules at specified time t that is positioned between specified distance, r and $r+dr$ which have velocities c and $c+Fdt$. For a system with no external forces, the Boltzmann transport equation can be simplified as.

$$\frac{\partial f}{\partial t} + c \cdot \nabla f = \Omega, \tag{2}$$

in which c is the particle velocity vector. The left hand side (LHS) of Eq. 2 represents the streaming step and the right hand term denotes the collision term, Ω. The underlying theory of LBM is based on the discrete Boltzmann equation. Due to the complicated collision term that exists in the RHS of the Boltzmann equation, it is difficult and burdensome to solve. To ease the computational effort, Bhatnagar, Gross and Krook

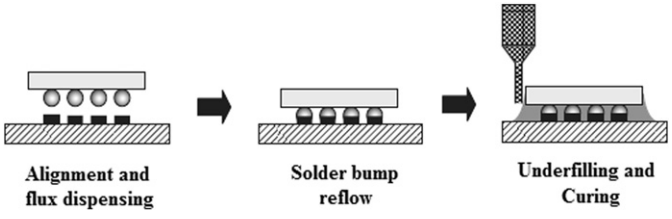

Fig. 2. Underfilling process flow.

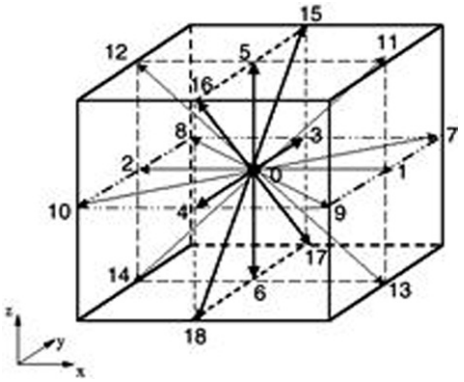

Fig. 3. 3D Lattice arrangements for D3Q19.

[24] proposed a simplified version of the collision operator. The collision operator can be replaced as

$$\Omega = \omega\left(f^{eq} - f\right) = \frac{1}{\tau}\left(f^{eq} - f\right) \tag{3}$$

where $\omega = \frac{1}{\tau}$. The coefficient ω denotes the collision frequency and τ is the relaxation factor. f^{eq} is the Maxwell–Boltzmann equilibrium distribution function. By substituting the approximate collision operator, the discrete Boltzmann equation along a specified direction can be shown as

$$\frac{\partial f_i}{\partial t} + c_i \cdot \nabla f_i = \frac{1}{\tau}\left(f_i^{eq} - f_i\right) \tag{4}$$

where i is the index selected between the possible discrete velocity directions and c_i is the particle velocity vectors along the discrete direction. The fluid density and macroscopic velocity can be found from the moment of the distribution function as below

$$\rho = \sum_i f_i^{eq} \tag{5}$$

$$u = \frac{1}{\rho}\sum_i f_i^{eq} c_i. \tag{6}$$

Subsequently, the equilibrium distribution, f^{eq}, can be arranged according to the Maxwell–Boltzmann distribution form as

$$f^{eq}(\rho, u) = \rho w\left[1 + \frac{1}{c_s^2}(c.u) + \frac{1}{2c_s^4}(c.u)^2 - \frac{1}{2c_s^2}(u.u)\right]. \tag{7}$$

Eq. 3 will replace the commonly used Navier–Stokes equation in CFD simulations. It is also possible to derive N–S equation from Boltzmann equation using the Chapman–Enskog model. For the case of D3Q19 lattice model as depicted Fig. 3 the weighting functions can be described in Table 1 as:

Microscopic velocities for a D3Q19 lattice model is given as:

$$e_0 = (0, 0, 0)$$

$$e_{1,2} = (\pm 1, 0, 0)$$

$$e_{3,4} = (0, \pm 1, 0)$$

$$e_{5,6} = (0, 0, \pm 1)$$

$$e_{7-10} = (\pm 1, \pm 1, 0)$$

$$e_{11-14} = (\pm 1, 0, \pm 1)$$

$$e_{15-18} = (\pm 1, 0, \pm 1). \tag{8}$$

Table 1
Weighting functions for D3Q19.

Model	c_s^2	Node no.	Weight
D3Q19	1/3	f_0	1/3
		f_1-f_6	1/18
		f_7-f_{18}	1/36

3.1.1. LBM pressure formulation

For single component multiphase (SCMP) flow, the pressure P can be described based on inter-particle forces from equation of state (EOS) as [26,27]

$$P = \rho RT + \frac{GRT}{2}[\psi(\rho)]^2 \tag{9}$$

where R is the universal gas constant, T is the temperature, G denotes the interaction strength and ψ is the interaction potential that can be represented as

$$\psi(\rho) = \psi_0 \, exp\left(-\frac{\rho_0}{\rho}\right) \tag{10}$$

with ψ_0 and ρ_0 are the arbitrary constants. This EOS model has been found effective and useful in the simulation of capillary phenomena and Laplace law problems [26].

3.1.2. LBM free-surface formulation

To track the flow propagation of epoxy mold, additional variable namely the volume of fraction ϵ is introduced based on the volume-of-fluid (VOF) formulation. The value of ϵ for the fluid and the gas cell can range between value of 0 and 1, respectively. The fluid mass content in a cell is calculated based on the volume of fraction ϵ and the density ρ as

$$M = \rho \cdot \epsilon. \tag{11}$$

3.2. Finite volume: Navier–Stokes formulation

In this paper, the governing equations based on Navier–Stokes equation are used to simulate the fluid flow of encapsulant material and air using the conservation of mass and momentum. In the encapsulation process, both fluids are assumed to be incompressible and laminar.

Continuity equation:

$$\frac{\partial \rho}{\partial t} + + \nabla.\left(\rho \vec{u}\right) = 0. \tag{12}$$

Navier–Stokes equation:

$$\frac{\partial}{\partial t}\left(\rho \vec{u}\right) + \nabla.\left(\rho \vec{u}\,\vec{u}\right) = -\nabla P + \nabla.\bar{\bar{\tau}} + \rho \vec{g}. \tag{13}$$

Energy equation:

$$\rho C_P\left(\frac{\partial T}{\partial t} + \vec{u}\nabla T\right) = \nabla(k\nabla T) + \Phi. \tag{14}$$

In the model, EMC and air are distinguished using multiphase formulation. The volume of fluids (VOF) for both phases is described using transport equation whilst the distribution of fluid is represented by volume fraction, f within the range of $0<f<1$. Generally, $f=0$ indicate the absence of EMC while $f=1$ indicate the cell is completely filled with EMC.

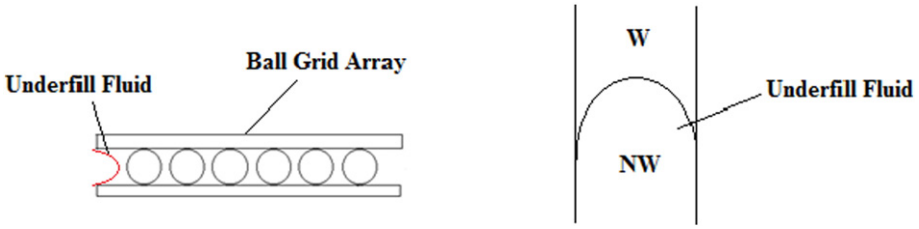

Fig. 4. Wetting and non-wetting region of underfill fluid.

Transport equation:

$$\frac{df}{dt} + \nabla.(\bar{u}\, f) = 0. \tag{15}$$

where $\vec{u}$ is the fluid velocity vector, ρ is the fluid density, P is the static pressure, T is the temperature, τ represents the stress tensor, k is the thermal conductivity, C_P is the specific heat and Φ represents the energy source.

3.3. Capillary force formulation

The underfill fluid flows through ball grid array (BGA) based on the capillary action without the assistance of the external force. There are two regions in the fluid capillary flow action which are wetting and non-wetting fluid region. The underfill fluid is in the non-wetting region as shown in Fig. 4.

The capillary pressure is defined as the pressure difference between wetting and non-wetting fluid. The equivalence to atmospheric pressure can be considered since the non-wetting fluid is air.

$$\Delta P_c = P_{nw} - P_w \tag{16}$$

$$\Delta P_c = \frac{2\sigma}{b} \tag{17}$$

where σ is the fluid surface tension and b is the gap height.

The Eqs. 15 and 16 show that capillary pressure is proportional to surface tension and inversely proportional to the gap height. There are two conditions as shown below:

$$\Delta P_c > \frac{2\sigma}{b} \tag{18}$$

The pressure of non-wetting fluid is greater than the pressure of the wetting fluid. Thus, the fluid in non-wetting region will fill or move to the wetting region (underfilling process phenomenon).

$$\Delta P_c < \frac{2\sigma}{b}. \tag{19}$$

The pressure of non-wetting fluid is lower than the pressure of the wetting fluid. Thus, the fluid in non-wetting region will remain static.

4. Multiphase formulation

The strongest attribute of LBM lies in its ability both single and multi-component multiphase fluids. The "component" term refers to chemical constituent, i. e. H_2O that can reside in either liquid or vapour phases. In this study we will use single component multiphase method (SCMP) to model the mould flow over solder bumps [25]. These San–Chen model is represented using the so called "pseudo potential force" as follows:

$$V\left(x, x'\right) = G\left(x, x'\right)\psi(x)\psi\left(x'\right) \tag{20}$$

where G is a Green's function and $\psi = \psi\,(p)$ is the "effective mass". The interaction force with the potential as given above can be written as

$$F = -G(|e_\alpha|)\psi(x)\sum_\alpha \psi(x + e_\alpha)e_\alpha. \tag{21}$$

Fig. 5 depicts the pseudo potential forces between inter-particles. The strength of interaction is controlled by the amplitude parameter G. Note that, positive G means attraction meanwhile negative G as repulsion. As a result, phase separation is determined by positive entries in the diagonal interaction matrix G and negative (repulsion) on the off-diagonal. It is noteworthy to mention that the air voids or bubble formation is highly dependent on these interaction strength. For most practical purposes, this interaction is described in its 'corral' form as

$$G(|e_\alpha|) = \begin{cases} G, & \text{if} |e_\alpha| = c, \\ 0, & if |e_\alpha| > c \end{cases} \tag{22}$$

where c is the lattice spacing. The velocity $u^{(eq)}$ is changed to $u + \tau F/\rho$ when the equilibrium distribution function is computed. The averaged momentum before and after collision is $\rho u + F/2$. The non-ideal gas equation of state (EOS) was specified by $\psi(\rho) = \rho_o[1 - \exp(-\frac{\rho}{\rho_o})]$.

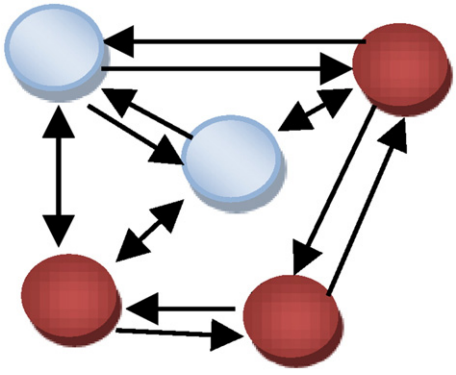

Fig. 5. The meaning of pseudo potential force. Each lattice population experiences an attractive force from colour-mate neighbours and a repulsive one from the opposite colour.

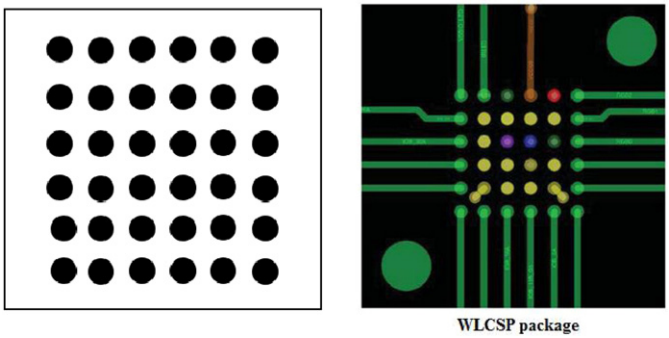

Fig. 6. 3D Full array BGA orientation.

Table 2
EMC encapsulant material properties.

Parameter	Value
Density (kg/m^3)	1042
Dynamics viscosity (Pa·s)	2.2
Kinematic viscosity (mm^2/s)	2111.3
Surface tension (N/m)	0.047
Bond number	1108

Analytical calculation can be computed to find the value of G and ρ, where the value of G is determined by the temperature. For the same fluid, the coexistence of two densities present at a range of ρ where dp/dρ is negative for the case that is below the critical values. The advantage of using this model is that phase segregation is generated automatically.

The trade-off however is that the collision operator does not conserve the momentum locally. Subsequently, the momentum is only conserve globally since there is no momentum exchanged at the boundaries.

5. Numerical simulation

A 3D IC package model was generated by using Palabos software that is based on the Lattice Boltzmann method (LBM) theory for simulating the fluid flow across ball array.

Fig. 6 depicts the full array BGA of the size, 6 × 6 array of solder balls that duplicates the model of 36 bump wafer level chip scale package (WLCSP), MXO3L-1300E-UWG36 and ICE5LP4K-SWG36. The geometry of simulation is depicted in Fig. 6. The flow is based entirely on capillary pressure with zero inlet velocity specified. Underfill material Hitachi CEL-9000 (LF) and air are defined in the analysis. Table 2 summarizes the material properties. Fig. 7 depicts the bottom and top surfaces in the left half of the channel that are shown with a bounce back boundary condition imposing a given static contact angle.

Periodic boundary conditions are imposed in the right half of the channel at top and bottom surfaces in order to model a "repeating" flow condition. Similarly, periodic boundary conditions are also imposed at the two lateral sides such to ensure total mass conservation inside the system [26]. At the solder bump surface, bounce back boundary conditions is used to model flow over obstacles [27]. As the name

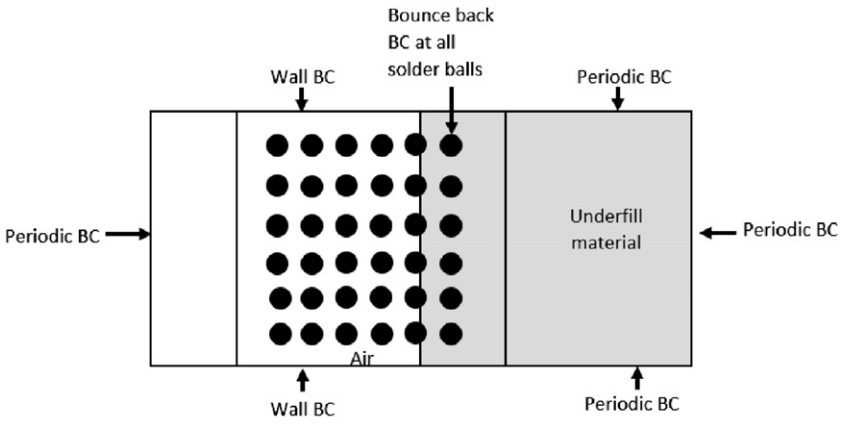

Fig. 7. LBM boundary conditions setup for periodic and bounce back conditions.

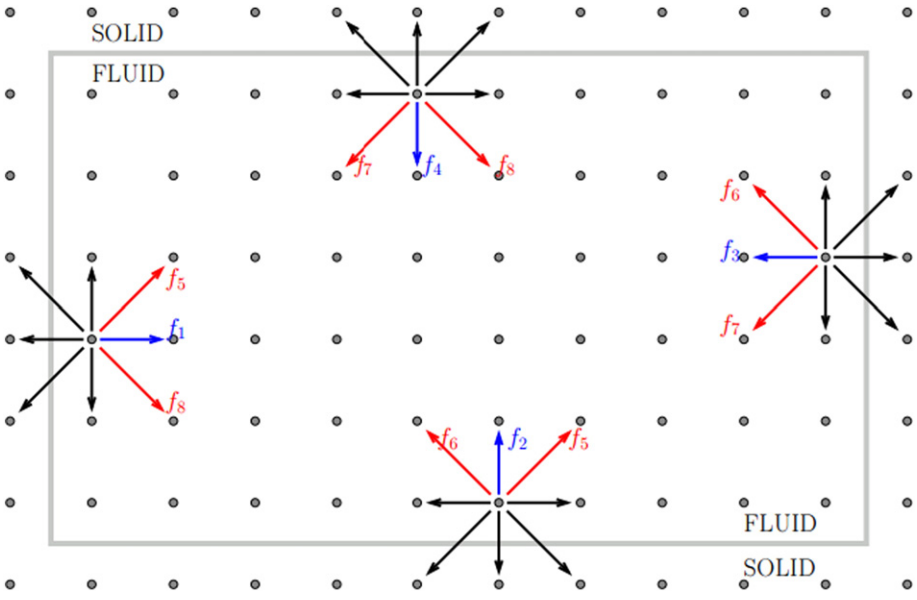

Fig. 8. LBM bounce back boundary conditions setup for flow over solder balls.

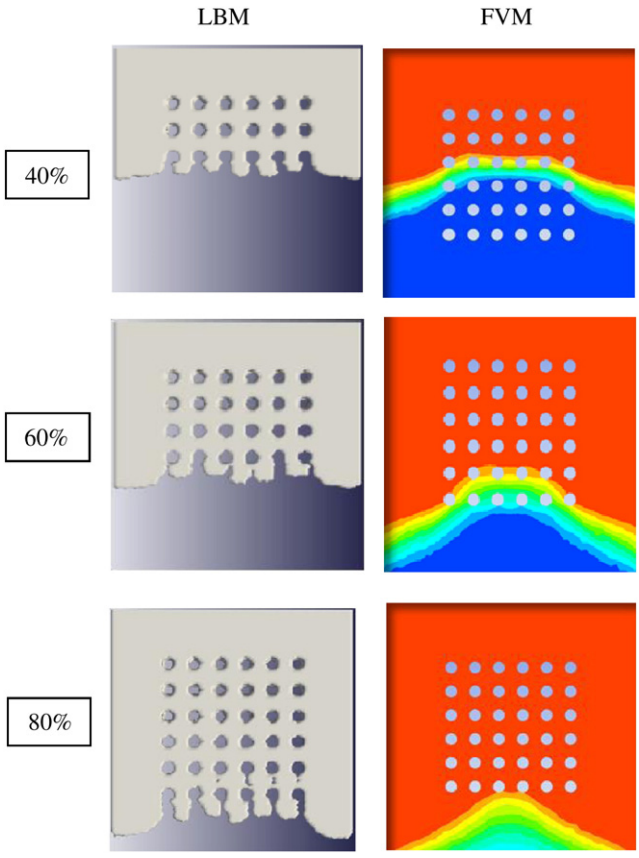

Fig. 9. Percentage of volume of fraction (VOF) contour at different filling time for full orientation.

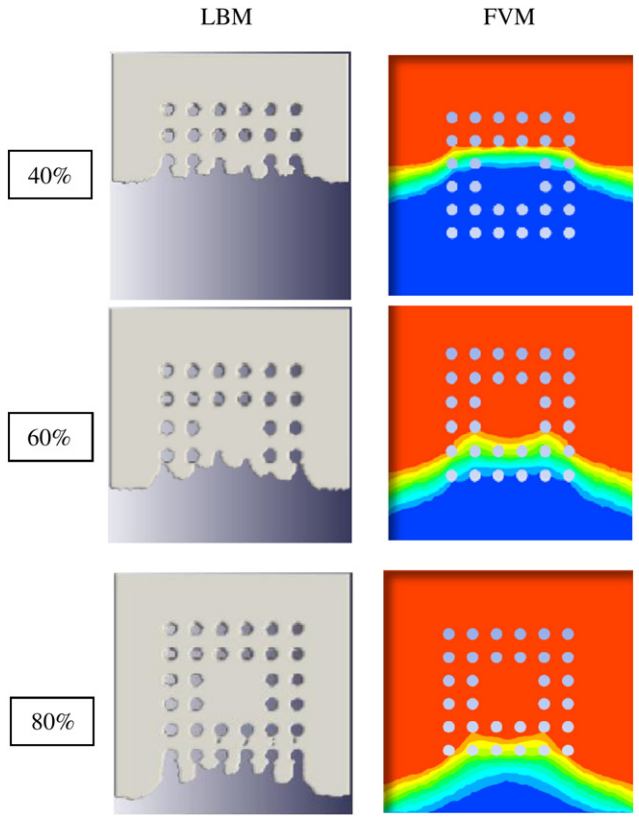

Fig. 10. Percentage of volume of fraction (VOF) contour at different filling time for middle empty orientation.

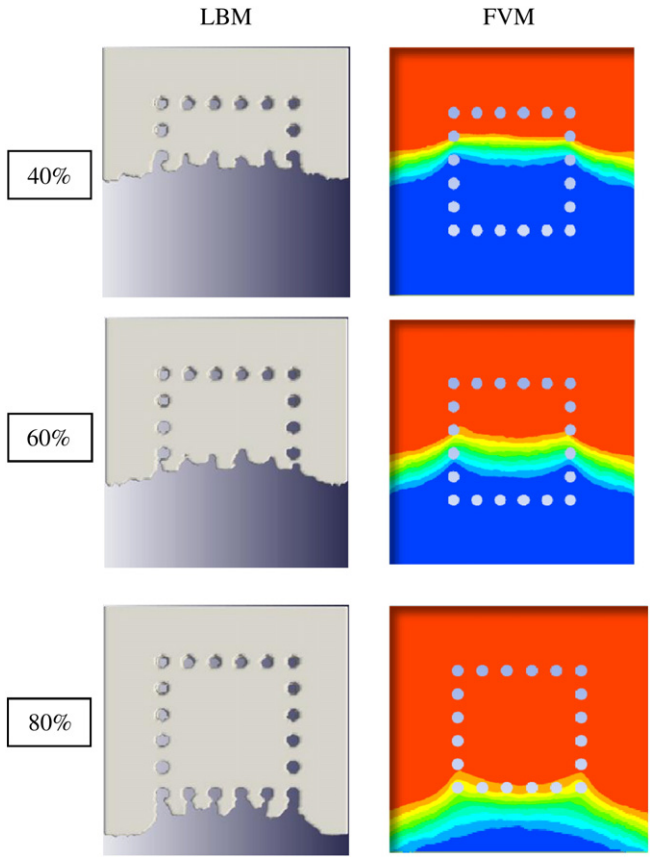

Fig. 11. Percentage of volume of fraction (VOF) contour at different filling time for middle empty orientation.

suggest, particles moving towards the solid boundary surface will bounce back in its original direction as depicted in Fig. 8.

6. Results and discussion

6.1. LBM and FVM void formation study

Void formation will lead to the reflow process issue and reduces the reliability of the encapsulated package. Void formation could lead to air traps inside the encapsulated package which will then vaporize into steam when high temperature occurs. This subsequently causes the interfacial loose or delamination. Delamination will then lead to the initial cracking which subsequently causes package failure.

For comparison, the filling time were assessed at different filling percentage for both LBM and FVM multiphase models. Figs. 9, 10 and 11 depict the multiphase flow front propagation at different filling percentages. At 40% flow, the location of air void formations can be clear for LBM simulations on all orientations compared to FVM models typically at the first row of solder bumps. This phenomenon is caused by reverse flow occurring at this location as a result of continuous flow at the inlet. At 80% filling, formation of air traps is highly visible using LBM models for middle empty and full orientations located before the end of the last row of solder bumps. Comparatively, the level of detail observed in LBM based software is better compared to FVM based software. The formation of bubble can be observed towards the end of 80% filling. This bubble could lead to localize stress concentration which in time leads to cracking at this area.

6.2. LBM multiphase flow at 100% filling

Fig. 12 shows the possible void formation location for all solder bump orientations using LBM based package. It was shown that middle

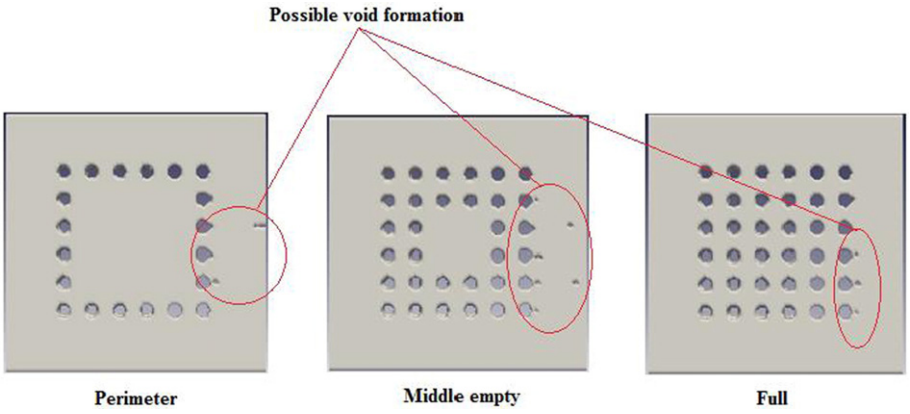

Fig. 12. Possible void formation for all orientations at 100% filling using LBM.

empty orientation shows the highest possible void formation compared to the full and perimeter orientation whereas the perimeter orientation has the least possible void formation. The middle empty orientation has the highest number of possible void formation due to the crowding of solder bumps that obstruct the fluid flow and the downward deformation of the center ball grid array (BGA) surface which restricted the flow. Besides, the possible void formation for all orientations is closer to the outlet which may be due to the decreasing value of velocity of the fluid flow with the flow front advancement and the solder bump obstruction. At the later part of BGA, the fluid flow with lower velocity will easily disperse by the solder bump. The dispersed fluid is difficult to recombine back after passing through solder bump due to high viscosity fluid property. In addition the possible void formation is concentrated at the middle part of the BGA rather than the edge of the BGA may due to unbalance flow front advancement (slower fluid flow at the middle and faster fluid flow at the edge of BGA).

This fluid flow with relatively lower velocity at the middle portion when in contact with the solder bumps could lead to flow front breakage that form voids.

6.3. Effect of pressure on void formation

Figs. 13, 14 and 15 show the pressure distribution of multiphase flow at the end of mould flow for all orientations. Based on Fig. 13, middle empty orientation shows the highest number of air void formation which is consistent with the results obtained by CY Khor [28] and Ernest [9]. Moreover, similar observation can be made on the location of air voids which is highly populated at the vicinity of microbumps near the inlet. Comparatively, more air void build up can be seen at the start of solder bump population. This is due to relatively high flow velocity since no contact with solder bump occurs at the start of the flow.

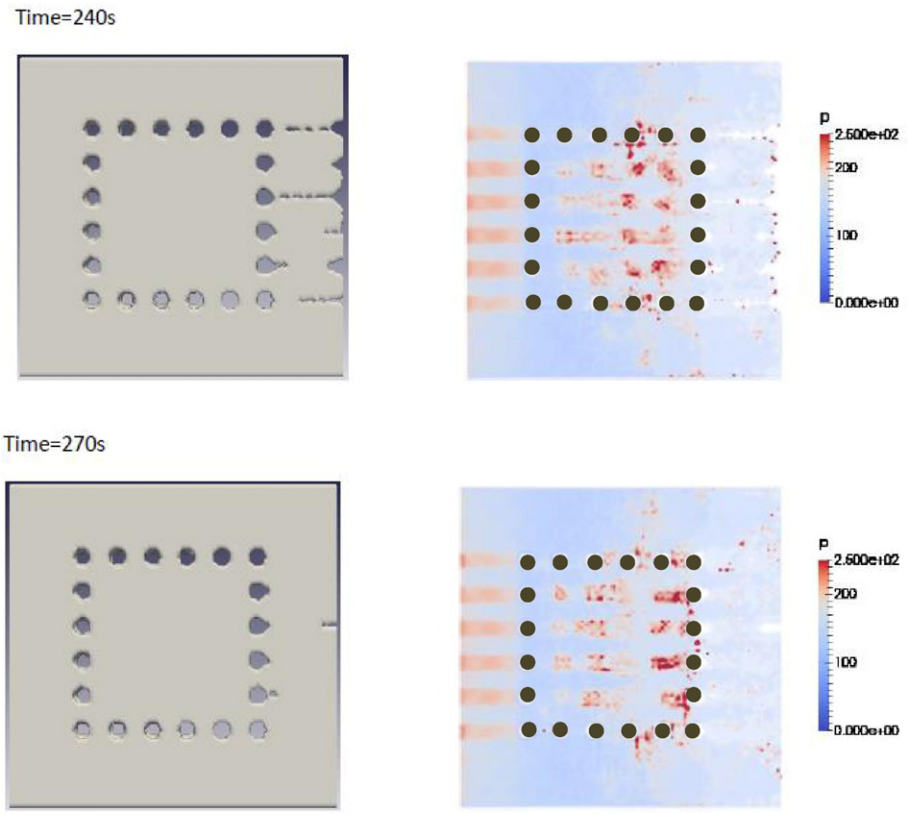

Fig. 13. Pressure distribution for perimeter orientation.

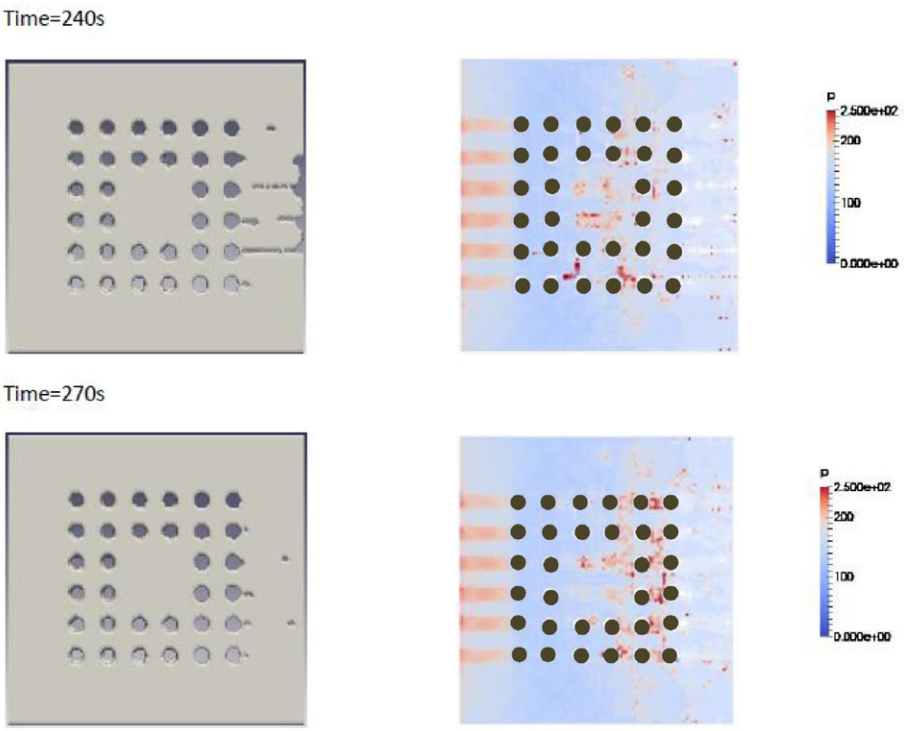

Fig. 14. Pressure distribution for middle empty orientation.

High pressure spots can be observed in Fig. 13 towards the end of the flow typically near the region when the two flows meet. The high pressure region reduces the possibility of void formation since the high pressure difference allows for much easier flow front to combine. Similar arguments can be made for full orientation with localized high pressure spots at the onset of air void formation. For the middle empty observation as depicted in Fig. 14, noticeable low pressure spots at the vicinity of air void formation resulted in smaller pressure difference at the end of flow. The melt front converges much harder compared to perimeter and huge amount of air void can be observed as shown in Fig. 13.

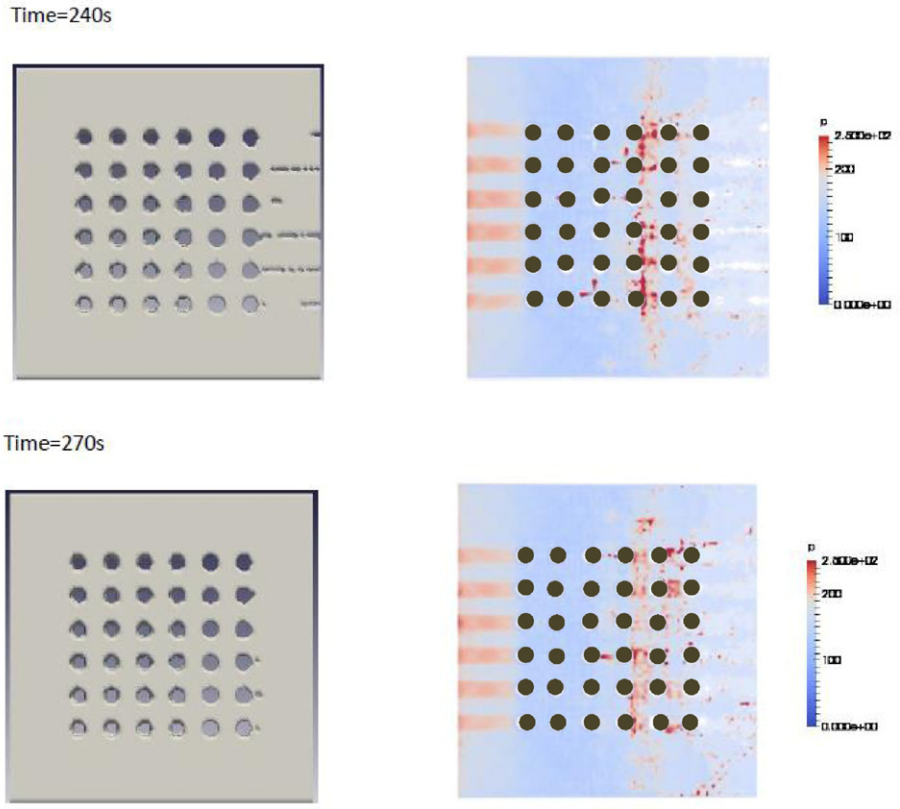

Fig. 15. Pressure distribution for full orientation.

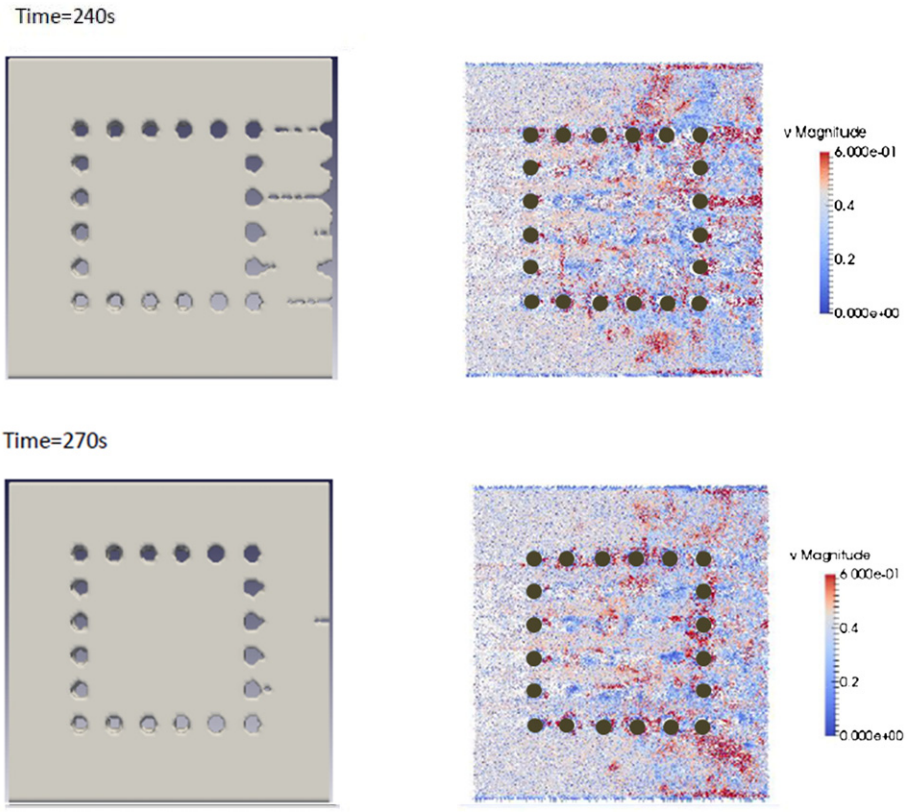

Fig. 16. Velocity distribution for perimeter orientation.

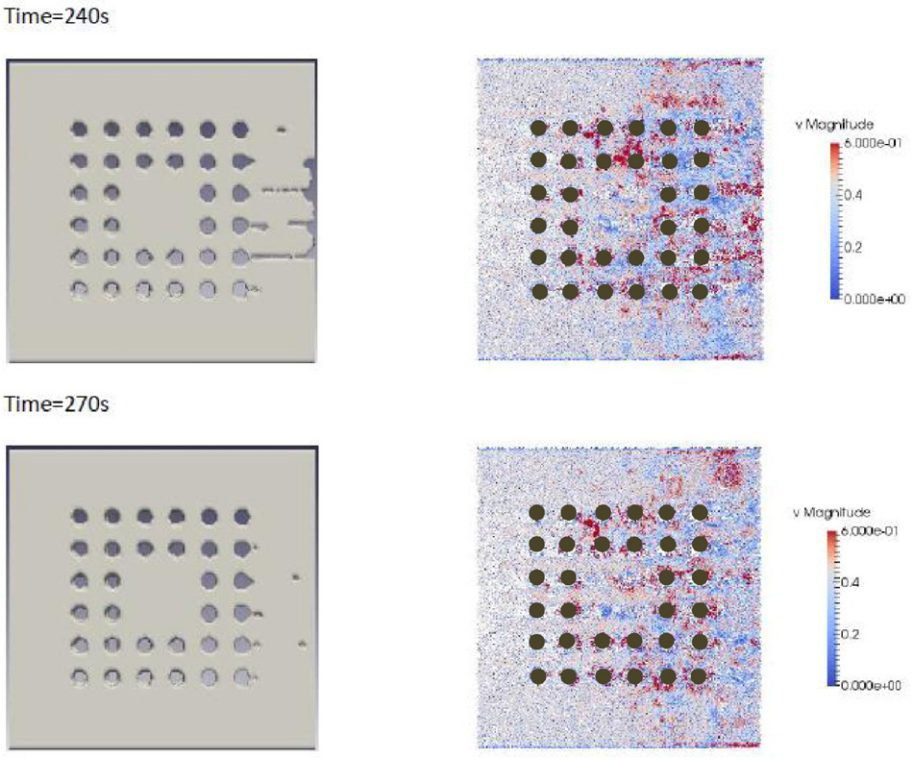

Fig. 17. Velocity distribution for middle empty orientation.

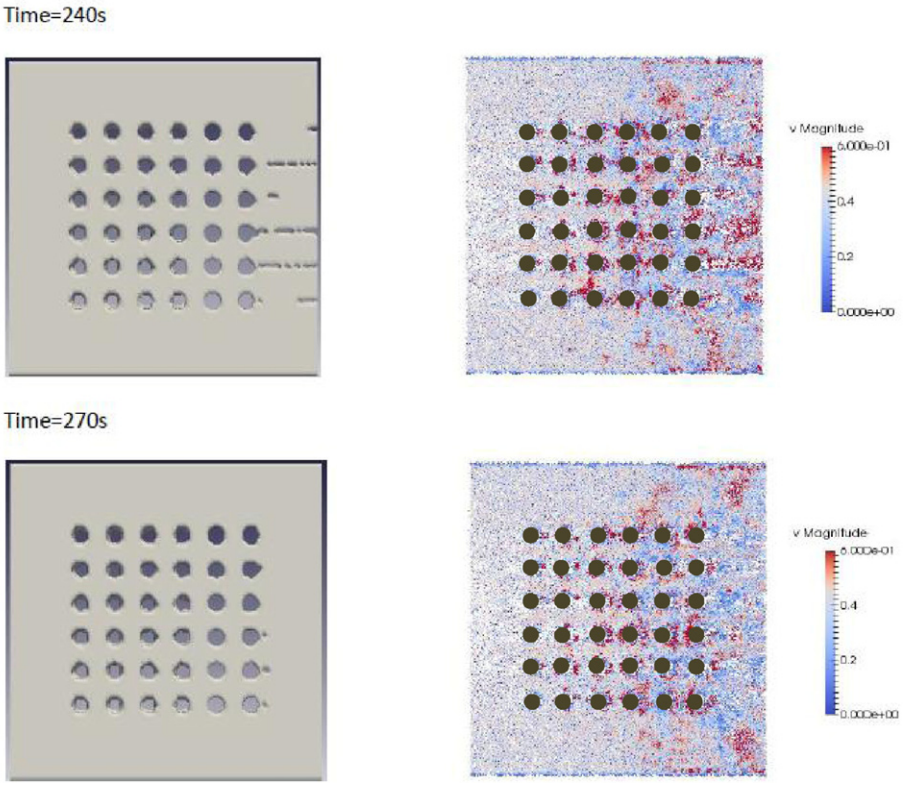

Fig. 18. Velocity distribution for full orientation.

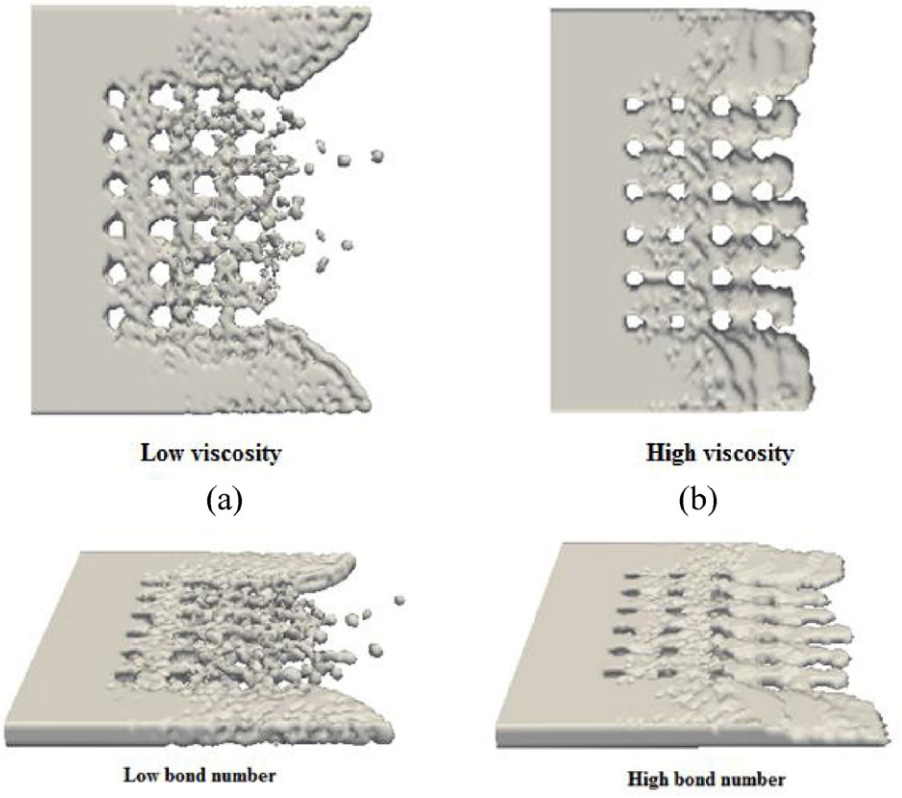

Fig. 19. Comparison between fluid flow with different viscosity and bond number.

6.4. Effect of velocity on void formation

The middle empty orientation as shown in Fig. 16 has relatively less high velocity spots at the center of bump free region compared to perimeter and full orientations. This slightly lower velocity regions result in slower converging flow front at the end of the flow. In addition, the racing effect phenomena also contributed to the air trap. The racing effect occurs due to obstruction of flow with the flow. The racing effect issue can be seen for all orientation as depicted in Figs. 16, 17 and 18 respectively. High velocity region is expected at the flow front surface during this racing effect. The racing effect combines with relatively slow flow rate can contribute in increasing the number of flow air traps.

6.5. Effect of bond number and viscosity on void formation

This section studies the effect of bond number and viscosity on the air void formation. Fluid flow behaviour depends on the viscosity and bond number of the fluid. Viscosity of a fluid measures its resistance to deformation due to stress. The fluid with a higher viscosity appears to be more solid. In contrast, the bond number (Bo) measures the significance of the surface tension forces compared to body forces in order to characterize the fluid flow pattern.

High value of bond number represents the system unaffected by surface tension whereas low value of bond number represents the system dominated by surface tension. Fig. 19 shows the comparison of fluid flow with different viscosities and bond numbers. Fig. 19(a) shows the epoxy mould flow with kinematic viscosity of 0.00001 mm^2/s and bond number of 100 whereas Fig. 19(b) is simulated with kinematic viscosity of 2111.3243 mm^2/s and bond number of 1108. From Fig. 19, fluid with lower viscosity has higher possibility of air trap since the particle–particle interaction forces are lower to prevent penetration of air in the mould. In terms of the bond number, high bond number has lower possibility of air traps. This is due to the mould has higher surface tension and penetration of air is more unlikely.

7. Conclusion

This paper shows the importance of solder bump arrangement in fluid flow filling time, pressure distribution and velocity distribution on the ball grid array (BGA). 3D models are created using both LBM and FVM formulations to predict the location of air void formation on capillary underfill I-type dispensing method for three different solder bump arrangements namely full, middle empty and perimeter orientations. The findings show good agreement between LBM and FVM in terms of filling percentage. However, in predicting the air void formation, LBM is able to accurately visualize the void formations better compared to FVM. It was shown that middle empty orientation has the highest number of air void followed by full and middle empty orientations. The air voids are concentrated at the vicinity of the first and final rows of the solder bumps. The former voids are caused by reverse flow phenomena located at the solder bumps nearest to the inlet while the latter voidformations are due to rapid change in flow rate moving from crowded solder bump region to bump-free region. To better visualize the factors leading to air void formation, the pressure and velocity of the multiphase flows are tracked at specified filling percentage. In general, non-uniform pressure is distributed throughout the underfill domain due to unbalanced fluid flow caused by lower flow rate at the bump free region. Perimeter orientation is shown to have highest pressure distribution followed by middle empty and full orientations as a result of this bump-free region. These high pressure spot could lead to package deformation due to pressure difference outside and inside underfill pressure. The results also show that for high pressure flow as shown in the middle empty orientation, air void formations are much harder. These high pressure spots lead to high pressure difference which in turn will increase the flow of the encapsulation. These findings are consistent with the velocity distribution which show low velocity spot typically for the middle empty configuration with higher number of air void compared to perimeter and full orientations. This lower velocity region combined with racing effect which occurs towards the end of the flow could lead to an increase in the number of air void formation. In reducing the effect of air void formation, the diameter of the solder bumps and its pitch dimension can be varied to reduce this air void formation caused by non-uniform pressure and velocity distributions. It was also shown that using high bond number and viscosity material could reduce the formation of air void and this factor could be accounted in finding appropriate underfill encapsulant mould. This study has shown the capability of LBM based software in simulating the real capillary underfill process and in the near future could prove vital as an alternative numerical tool for 3D multiphase flow problems.

Acknowledgements

The work was partly supported by the Short Term Grant 60313020 from the Division of Research and Innovation, Universiti Sains Malaysia.

References

[1] J.J. Liu, H. Berg, Y. Wen, S. Mulgaonker, R. Bowlby, A. Mawer, Plastic ball grid array (PBGA) overview, Mater. Chem. Phys. 40 (1995) 236–244.
[2] P.S. Ho, G. Wang, M. Ding, J.H. Zhao, X. Dai, Reliability issues for flip-chip packages, Microelectron. Reliab. 44 (2004) 719–737.
[3] W.H. Zhong, Y.C. Chan, M.O. Alam, B.Y. Wu, J.F. Guan, Effect of multiple reflow processes on the reliability of ball grid array (BGA) solder joints, J. Alloys Compd. 414 (2006) 123–130.
[4] R. Gannamani, M. Pecht, An experimental study of popcorning in plastic encapsulated microcircuits, IEEE Trans. Compon. Packag. Manuf. Technol. Part A: 19 (1996) 194–201.
[5] H. Ardebili, M.G. Pecht, Encapsulation Technologies for Electronic Applications, Elsevier, 2009.
[6] Z. Song, D. Wu, H. Zhu, L. Liu, Z. Wang, Void-formation in uncured and partially-cured BCB bonding adhesive on patterned surfaces, Microelectron. Eng. 137 (2015) 164–168.
[7] E.E.S. Ong, M.Z. Abdullah, C.Y. Khor, W.K. Loh, C.K. Ooi, R. Chan, Fluid–structure interaction analysis on the effect of chip stacking in a 3D integrated circuit package with through-silicon vias during plastic encapsulation, Microelectron. Eng. 113 (2014) 40–49.
[8] C.Y. Khor, M.Z. Abdullah, C.S. Lau, W.C. Leong, M.S. Abdul Aziz, Influence of solder bump arrangements on molded IC encapsulation, Microelectron. Reliab. 54 (2014) 796–807.
[9] E.E.S. Ong, M.Z. Abdullah, C.Y. Khor, W.C. Leong, W.K. Loh, C.K. Ooi, et al., Numerical modeling and analysis of microbump pitch effect in 3D Ic package with Tsv during molded underfill (Muf), Eng. Appl. Comput. Fluid Mech. 7 (2013) 210–222.
[10] C.Y. Khor, M.Z. Abdullah, M.K. Abdullah, M.A. Mujeebu, D. Ramdan, M.F.M.A. Majid, et al., Numerical analysis on the effects of different inlet gates and gap heights in TQFP encapsulation process, Int. J. Heat Mass Transf. 54 (2011) 1861–1870.
[11] B. Chopard, M. Droz, Cellular Automata Modeling of Physical Systems, 2005 (https://books.google.com.my/books?id=jfcxaoNZuMUC).
[12] P. Papatzacos, Cellular Automaton Model for Fluid Flow in Porous Media, Com. Plex Syst. 3 (1989) 383–405 (http://www.complex-systems.com/pdf/03-4-5.pdf).
[13] X. Shan, H. Chen, Lattice Boltzmann model for simulating flows with multiple phases and components, Phys. Rev. E 47 (1993) 1815–1819.
[14] X. Shan, H. Chen, Simulation of nonideal gases and liquid–gas phase transitions by the lattice Boltzmann equation, Phys. Rev. E 49 (1994) 2941–2948.
[15] X. Shan, G.D. Doolen, Diffusion in a multicomponent lattice Boltzmann equation model, Phys. Rev. E Stat. Phys. Plasmas Fluids Relat. Interdiscip. Topics 54 (1996) 3614–3620 (http://www.ncbi.nlm.nih.gov/pubmed/9965509).
[16] M.R. Swift, W.R. Osborn, J.M. Yeomans, Lattice Boltzmann simulation of nonideal fluids, Phys. Rev. Lett. 75 (1995) 830–833.
[17] L.-S. Luo, Some Recent Results on Discrete Velocity Model and Ramifications for Lattice Boltzmann Equation, 2000.
[18] X. He, G.D. Doolen, Thermodynamic foundations of kinetic theory and Lattice Boltzmann models for multiphase flows, J. Stat. Phys. 107 (2002) 309–328.
[19] J. Zhang, D.Y. Kwok, Lattice Boltzmann study on the contact angle and contact line dynamics of liquid–vapor interfaces, Langmuir 20 (2004) 8137–8141.
[20] R. Zhang, H. Chen, Lattice Boltzmann method for simulations of liquid–vapor thermal flows, Phys. Rev. E Stat. Nonlinear Soft Matter Phys. 67 (2003) 066711.
[21] X. Shan, G. Doolen, Multicomponent Lattice-Boltzmann model with interparticle interaction, J. Stat. Phys. 81 (1995) 379–393.
[22] X. Shan, H. Chen, Simulation of nonideal gases and liquid–gas phase transitions by the Lattice Boltzmann equation, Phys. Rev. E 49 (1994) 2941–2948.
[23] C. Bailey, Numerical modelling for electronic packaging — future requirements, 2005 6th Int, Conf. Electron. Packag. Technol. 5–6 (2005).

[24] P.L. Bhatnagar, E.P. Gross, M. Krook, A model for collision processes in gases. I. Small amplitude processes in charged and neutral one-component systems, Phys. Rev. 94 (1954) 511–525.
[25] A.K. Gunstensen, D.H. Rothman, S. Zaleski, G. Zanetti, Lattice Boltzmann model of immiscible fluids, Phys. Rev. A 43 (1991) 4320–4327.
[26] M.C. Sukop, D. Or, Lattice Boltzmann method for modeling liquid–vapor interface configurations in porous media, Water Resour. Res. 40 (2004).
[27] A.A. Mohammed, Lattice Boltzmann Method: Fundamentals and Engineering Applications with Computer Codes, Springer, New York, 2012.
[28] C.Y. Khor, M.Z. Abdullah, Z.M. Ariff, W.C. Leong, Effect of stacking chips and inlet positions on void formation in the encapsulation of 3D stacked flip-chip package, Int. Commun. Heat Mass Transfer 39 (2012) 670–680.